FINE-GRAINED CONTRASTIVE LEARNING FOR ECG-REPORT ALIGNMENT WITH WAVEFORM ENHANCEMENT

Anonymous authors
Paper under double-blind review

ABSTRACT

Electrocardiograms (ECGs) are essential for diagnosing cardiovascular diseases. However, existing ECG-Report contrastive learning methods focus on whole-ECG and report alignment, missing the link between local ECG features and individual report tags. In this paper, we propose FG-CLEP (Fine-Grained Contrastive Language ECG Pre-training), which achieves fine-grained alignment between specific ECG segments and each tag in the report via tag-specific ECG representations. Furthermore, we found that nearly 55% of ECG reports in the MIMIC-ECG training dataset lack detailed waveform features, which hinders fine-grained alignment. To address this, we introduce a coarse-to-fine training process that leverages large language models (LLMs) to recover these missing waveform features and validate the LLM outputs using a coarse model. Additionally, fine-grained alignment at the tag level, rather than at the report level, exacerbates the false negative problem, as different reports may share common tags. To mitigate this, we introduce a semantic similarity matrix to guide the model in identifying and correcting false negatives. Experiments on six datasets demonstrate that FG-CLEP significantly improves fine-grained alignment, outperforming state-of-the-art methods in both zero-shot prediction and linear probing. Meanwhile, the fine-grained reports we generate also enhance the performance of other methods. Our code and data are available at: https://anonymous.4open.science/r/FG-CLEP-3454.

1 INTRODUCTION

Electrocardiograms (ECGs) are essential non-invasive tools for detecting cardiac rhythm disorders in clinical practice (Sahoo et al., 2020; Rath et al., 2021; Ayano et al., 2022). Recently, self-supervised learning (SSL) has emerged as a promising paradigm for ECG representation learning, alleviating the reliance on large-scale annotated data and expert knowledge. Existing ECG SSL approaches can be broadly categorized into comparative methods (Chen et al., 2020; 2021; Wang et al., 2023; Eldele et al., 2021) and generative methods (Zhang et al., 2022a; Hu et al., 2023; Na et al., 2024; Zhang et al., 2022b). However, most of these methods still struggle with unseen classes in zero-shot scenarios.

Inspired by the success of multimodal contrastive learning such as CLIP (Radford et al., 2021), recent studies have explored ECG–report alignment to enable zero-shot prediction. For instance, Li et al. (2024); Liu et al. (2024a); Lalam et al. (2023) align ECG signals with paired textual reports, while MERL (Liu et al., 2024b) enhances such representations with uni-modal alignment and descriptive prompts from LLMs. ESI (Yu et al., 2024) further integrates retrieval-augmented generation (RAG) (Ni et al., 2025; Gao et al., 2023) pipelines to enrich ECG reports with external medical knowledge. These efforts demonstrate the potential of ECG–text alignment for zero-shot learning.

Despite recent advances, current methods predominantly focus on aligning entire ECGs with their corresponding reports, neglecting the fine-grained relationship between local ECG features and individual report tags. To achieve fine-grained alignment, we identify and address three key challenges.

1.Fine-grained Alignment Architecture: Most existing approaches align entire ECGs with whole reports, but they fail to capture patch-level ECG embeddings and tag-specific report embeddings, both of which are critical for fine-grained alignment.

2.Missing Waveform Features in Reports: We observe that nearly 55% of ECG reports in the MIMIC-ECG dataset—one of the largest ECG-Report datasets—lack detailed waveform features, which hampers fine-grained alignment. In clinical practice, physicians often begin by identifying key waveform patterns in an ECG before formulating a diagnosis. However, many physicians do not explicitly record these features in the reports, resulting in a significant portion of reports lacking important waveform information. Recovering these missing features using large language models (LLMs) is challenging for two main reasons: (1) the hallucination problem inherent in LLMs (Huang et al., 2023; Günay et al., 2024; Zhang et al., 2025), and (2) the non-bijective relationship between waveform features and diagnostic outcomes, where the same disease may manifest with different waveform patterns (Jin, 2018). As a result, relying solely on LLMs to augment reports, as attempted by Yu et al. (2024), proves to be unreliable.

3.False Negative Challenge: Fine-grained alignment at the tag level, rather than at the report level, exacerbates the false negative problem. This is because different reports may share common tags, leading to potential misalignments.

In this study, we propose FG-CLEP to address the aforementioned challenges. Rather than aligning the entire ECG embedding with the report embedding, we perform alignment at the ECG patch level and the individual tag level in the report. Specifically, we obtained tag-specific ECG representations, where different tags in the report serve as queries to attend to ECG patches (treated as keys and values) through cross-attention. To address missing waveform features in reports and generate fine-grained reports, we propose a coarse-to-fine training process. First, we train a coarse CLEP model using contrastive learning on the original ECG-report pairs. Then, we use LLMs to generate potential waveform features from the reports, which are validated using CLEP. Finally, we integrate these validated features into the reports and continue training the CLEP model to obtain the final FG-CLEP model. This approach resolves the non-bijective relationship between waveform features and diagnoses and corrects errors from LLM hallucinations. Lastly, to address the false negative problem exacerbated by fine-grained tag-level alignment, we introduce a semantic similarity matrix. This matrix computes the similarity between tags and is used during contrastive learning to guide the model in identifying and correcting false negatives.

We validate our proposed FG-CLEP on six ECG multi-label classification datasets in both zero-shot and linear probing, the results demonstrate that FG-CLEP significantly improves fine-grained alignment, outperforming state-of-the-art methods in both zero-shot prediction and linear probing. Meanwhile, the fine-grained reports we generate also enhance the performance of other methods. Overall, our contributions are threefold:

- We propose a new alignment architecture, enabling fine-grained alignment between ECG segments and report tags through tag-specific ECG representations, capturing detailed ECG-report relationships.
- We introduce a coarse-to-fine training process using LLMs to recover missing waveform features and validate them with a coarse CLEP model, addressing non-bijective relationships and LLM hallucinations.
- We present a semantic similarity matrix to mitigate false negatives in ECG-tag pairs, guiding contrastive learning to correct misalignments.
- Experimental results show that FG-CLEP, pre-trained on MIMIC-ECG, outperforms state-of-the-art methods in zero-shot prediction and linear probing across six datasets, including PTB-XL, CPSC2018, and CSN.

2 Related Work

ECG-Report Contrastive Learning Recently, inspired by the strong zero-shot ability of image-caption multimodal contrastive learning methods like CLIP (Radford et al., 2021), significant efforts have been made in ECG-Report contrastive learning (Li et al., 2024; Liu et al., 2024b;a; Yu et al., 2024; Lalam et al., 2023). Similar to CLIP (Radford et al., 2021), Li et al. (2024); Liu et al. (2024a); Lalam et al. (2023); Wang et al. (2025); Pham et al. (2024) learns ECG representations by pulling ECGs with their paired reports while pushing them from unpaired reports. MERL (Liu et al., 2024b) further introduces uni-modal alignment and employs the CKEPE pipeline at inference to generate more descriptive prompts via LLMs. However, enhancing textual prompts only during

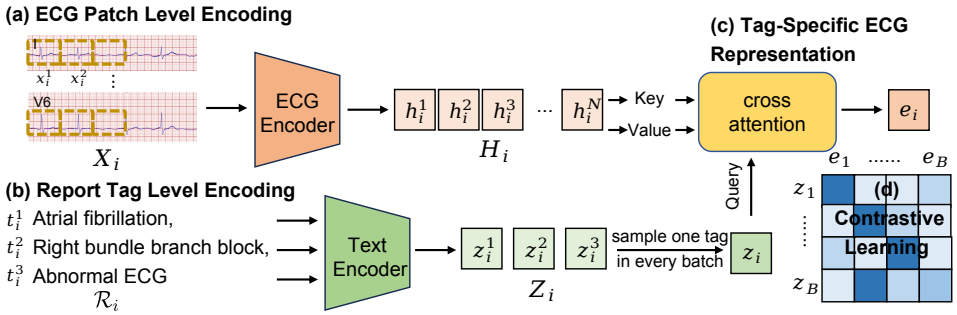

Figure 1: Fine-grained Alignment Architecture with Tag-Specific ECG Representation.

inference creates a distribution mismatch between training and testing text. In contrast, ESI (Yu et al., 2024) enhances ECG reports during training using a retrieval-augmented generation (RAG) pipeline, integrating LLMs and external medical knowledge for more detailed descriptions.

Despite these advances, existing methods all perform contrastive learning at the whole-ECG and report level, and overlook the absence of fine-grained waveform features in ECG reports. To address these challenges, we propose the FG-CLEP.

Fine-Grained Contrastive Learning Recent studies in medical imaging have demonstrated the benefits of fine-grained alignment. Methods such as MedFILIP (Liang et al., 2025), fVLM (Shui et al., 2025) incorporate entity-level or region-level supervision by leveraging structured information extracted from reports or by segmenting images into anatomical regions. These approaches enable more precise matching between local visual features and textual descriptions, resulting in improved downstream performance, especially in zero- and few-shot settings.

However, the application of fine-grained contrastive learning in the ECG domain remains largely unexplored. To bridge this gap, we propose to model fine-grained correspondences between characteristic ECG waveform segments and specific textual patterns in the reports, aiming to capture subtle diagnostic cues that may be overlooked in global-level alignment.

False Negatives in Contrastive Learning Traditional multi-modal contrastive learning (Radford et al., 2021) assumes that only images and captions from the same record are positive pairs. However, this assumption often fails in the ECG domain, where most ECGs are normal, and abnormalities typically involve common diseases, leading to frequent false negatives. Furthermore, fine-grained alignment at the tag level exacerbates this issue, as different reports may share common tags. There have been several attempts to address this issue (Lavoie et al., 2024; Jiang et al., 2023b; Sun et al., 2023; Li et al., 2023; Kim et al., 2025). Some approaches (Jiang et al., 2023b; Li et al., 2023) attempt to add a regularization term to mitigate false negatives. Others (Sun et al., 2023; Wang et al., 2022) introduce a matrix to measure the similarity between different reports, guiding contrastive learning to identify and address false negatives. In this paper, fine-grained alignment introduces a more pronounced false negative problem, as different reports may share common tags.

3 Method

3.1 Fine-Grained Alignment

In this section, we describe how we achieve fine-grained alignment between specific ECG segments and tags in clinical reports. Given an ECG-report dataset $\mathcal{D} = \{(\mathbf{X}_i, \mathcal{R}_i)\}_{i=1}^{M}$, each report $\mathcal{R}_i$ consists of multiple clinically meaningful tags, such as *arrhythmia*, *myocardial infarction*, *atrial fibrillation*, etc. For each tag, our objective is to identify and align the corresponding ECG segment(s) that reflect this clinical finding. To achieve this, we first perform **ECG patch-level encoding** and **report tag-level encoding** to obtain fine-grained representations of both the ECG signals and the report tags.

ECG Patch-Level Encoding. To obtain fine-grained ECG representations, we employ ViT to encode patch-level features from the ECG signal. Given a 12-lead ECG $\mathbf{X}_i \in \mathbb{R}^{L \times T}$, where $L = 12$ is the number of leads and T is the signal length, we independently divide each lead into N_{lead} non-

overlapping segments (patches) along the temporal axis, with each patch of length $\Delta T = T/N_{\text{lead}}$. This yields a total of $N = L \times N_{\text{lead}}$ patches:

$$\mathbf{X}_i \to \{\mathbf{x}_i^p\}_{p=1}^{N}, \quad \mathbf{x}_i^p \in \mathbb{R}^{1\times\Delta T}. \tag{1}$$

All N patches are passed through the ECG encoder resulting in a sequence of patch-level embeddings:

$$\mathbf{H}_i = \left[\mathbf{h}_i^1, \ldots, \mathbf{h}_i^N\right] = \text{ECGEncoder}\left(\left[\mathbf{x}_i^1, \ldots, \mathbf{x}_i^N\right]\right) \in \mathbb{R}^{N\times d}. \tag{2}$$

Report Tag-Level Encoding. Since ECG reports are highly structured, we can simply use commas to split the tags. We denote the set of tags in the i-th report as $\mathcal{T}_i = \{t_i^j\}_{j=1}^{m_i}$, where t_i^j represents the j-th tag in report i, and m_i is the number of tags in $\mathcal{R}_i$. Each tag t_i^j is then independently encoded via a text encoder to obtain its embedding representation. This yields the tag-level representation matrix for report i:

$$\mathbf{Z}_i = [\mathbf{z}_i^1, \ldots, \mathbf{z}_i^{m_i}] \in \mathbb{R}^{m_i\times d}, \tag{3}$$

$$\mathbf{z}_i^j = \text{TextEncoder}(t_i^j), \quad j = 1, \ldots, m_i. \tag{4}$$

Notably, both the ECG patch embeddings and tag embeddings are projected into the same latent space with dimension d. For clarity and conciseness, we omit explicit projection formulas in the equations above.

Tag-Specific ECG Representation. With the above fine-grained ECG patch embeddings and report tag embeddings, we can now align them at a fine-grained level. Ideally, if explicit annotations mapping each tag to its corresponding ECG patches were available, direct supervised alignment could be applied. However, such fine-grained annotations are typically unavailable in practice. To address this, we propose an automatic alignment mechanism based on cross-attention.

Specifically, for each tag, we use its embedding as the query and the ECG patch embeddings as keys and values. Through the cross-attention mechanism, the model adaptively computes a tag-specific ECG representation by attending to ECG patches according to their relevance to the tag. This enables each tag to aggregate information from the most relevant ECG segments, capturing the fine-grained relationship without requiring extra supervision.

Formally, given a tag embedding $\mathbf{z}_i^j$ and ECG patch embeddings $\mathbf{H}_i$, we compute the tag-specific ECG representation as:

$$\mathbf{e}_i^j = \text{CrossAttn}(\mathbf{z}_i^j, \mathbf{H_i}) = \sum_{p=1}^{N} \alpha_{j,p} \cdot \mathbf{h}_i^p, \tag{5}$$

$$\alpha_{j,p} = \frac{\exp(\langle \mathbf{z}_i^j, \mathbf{h}_i^p \rangle)}{\sum_{p'=1}^{N} \exp(\langle \mathbf{z}_i^j, \mathbf{h}_i^{p'} \rangle)}. \tag{6}$$

Fine-Grained Contrastive Learning Objective. For each random batch with size B, we sample one tag z_i from each report's tag set $\mathbf{Z}_i$, and compute its corresponding tag-specific ECG representation $\mathbf{e}_i$. The learning objective is to maximize the similarity between each tag embedding and its corresponding ECG representation, while minimizing the similarity with unpaired ones, similar to SigLIP (Zhai et al., 2023) for its efficiency compared to the original CLIP.

$$L_{\text{con}} = -\frac{1}{B}\sum_{i=1}^{B}\sum_{j=1}^{B} \log\left(\frac{1}{1+\exp\left(-y_{ij}\cdot t\cdot \text{sim}(\mathbf{e}_i, \mathbf{z}_j)\right)}\right). \tag{7}$$

where y_{ij} denotes the match between a given ECG and report input(1 if i==j, otherwise -1), $\text{sim}(\cdot,\cdot)$ denotes the cosine similarity, and t is a temperature hyperparameter.

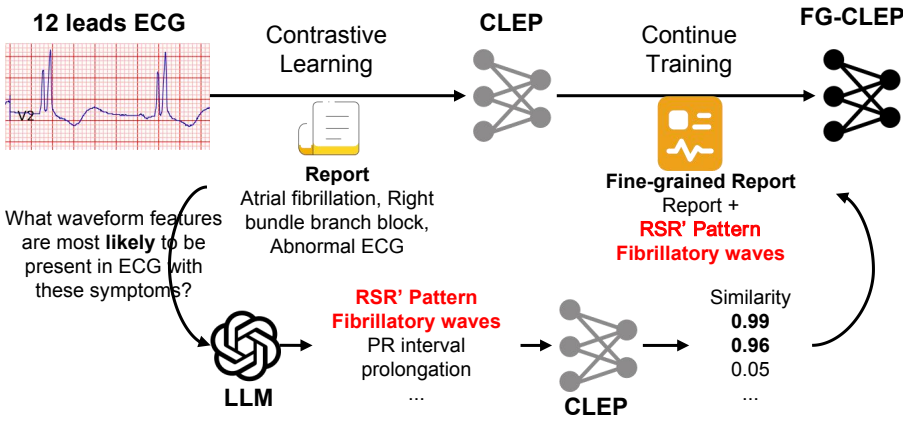

Figure 2: **Coarse-to-Fine Training Process of FG-CLEP.** The reports with recovered waveform features are referred to as fine-grained reports. Models trained with fine-grained reports are prefixed with FG-.

3.2 Coarse-to-Fine Training Process

Fine-grained alignment relies on fine-grained reports that include detailed waveform features. Although we achieve fine-grained alignment between tags and specific ECG segments, as discussed above, we observe that due to clinical habits, nearly half of the reports do not record waveform features as intermediate observations. Therefore, we propose a novel training process illustrated in Figure 2 consisting of three steps: (1) training the CLEP model using contrastive learning on original ECG-report pairs, (2) generating potential waveform features based on the original report using LLMs and validating them with CLEP, and (3) continuing to train the CLEP model with this augmented report containing waveform features to obtain the final FG-CLEP model.

The key to our training process is to recover the missing waveform features in the report. Given a report, we query LLMs with the question, *'What waveform features are most likely to be present in electrocardiograms with these symptoms?'* to identify potential overlooked waveform features. To format the results, we further instruct, *'Organize these waveform features into a Python list, with each item representing a distinct waveform feature.'* Using this explicit chain-of-thought instruction (Wei et al., 2022), we obtain a list of potential waveform features. However, LLM outputs are unreliable for two reasons: First, ECG waveform features and diagnoses are not in a one-to-one correspondence (Jin, 2018)—a single disease may present different waveform characteristics across individuals. Doctors can infer a diagnosis from waveform features, but not the other way around. Second, even if the non-bijective relationship is excluded, the LLM's output is inherently unstable due to hallucination issues (Huang et al., 2023; Günay et al., 2024).

Thus, we validate LLM-generated waveform features by computing their similarity to the ECG signal using coarse CLEP, selecting only high-confidence waveform features for augmentation. These validated features are then incorporated into the original report for continued training of the Fine-Grained CLEP model.

3.3 False Negative Mitigation

To address the false negative problem exacerbated by tag-level fine-grained alignment, we introduce a semantic similarity matrix that computes the similarity between different tags. This matrix is incorporated into contrastive learning to guide the model in identifying and correcting false negatives.

Formally, the semantic similarity matrix $\mathbf{S} \in \mathbb{R}^{B \times B}$ is defined as follows.

$$\mathbf{S}_{ij} = \text{sim}(\mathbf{e}_i, \mathbf{e}_j) \in [0, 1]. \tag{8}$$

We integrate the semantic similarity matrix into the loss function to guide contrastive learning, following the approach in (Sun et al., 2023). This matrix captures the semantic similarity between tags from different reports, enabling the model to identify and correct false negative samples by ensuring that similar tags are aligned more effectively, even if they belong to different reports.

The loss term L_{fnm} is defined as:

$$L_{\text{fnm}} = \frac{1}{B}\sum_{i=1}^{B}\sum_{j=1}^{B}\left|\text{sim}(\mathbf{e}_i, \mathbf{z}_j) - \mathbf{S}_{ij}\right|. \tag{9}$$

where B is the batch size and $|\cdot|$ denotes the L1 distance.

The final loss function for FG-CLEP is the combination of the contrastive loss and the false negative mitigation loss:

$$L = L_{\text{con}} + \lambda L_{\text{fnm}}. \tag{10}$$

4 EXPERIMENTS

4.1 DATASETS

We pre-train the FG-CLEP framework using the MIMIC-ECG (Gow et al.) dataset and test it on the PTB-XL (Wagner et al., 2020), CPSC2018 (Liu et al., 2018), and CSN (Zheng et al., 2022) datasets, following the benchmark proposed by (Liu et al., 2024b). All the ECGs in the datasets are 12-lead recordings. The MIMIC-ECG dataset contains nearly 800,000 ECG-report pairs. To improve data quality, we excluded samples with an empty report or reports containing fewer than three words, removed reports without useful information, and discarded ECGs with unexpected situations. Details regarding the train:validation:test split and other dataset-specific information are provided in the Appendix.

4.2 IMPLEMENTATION DETAILS

Pre-training Implementation: In the pre-training stage, we utilize a randomly initialized ViT model (Dosovitskiy et al., 2020) as the ECG encoder and BioClinicalBERT (Alsentzer et al., 2019) for text encoding. The whole ECG is divided into 60 non-overlapping patches. The AdamW optimizer is selected with a learning rate of 2×10^{-5} and a weight decay of 1×10^{-4}. CLEP is pre-trained for 10 epochs with original reports and FG-CLEP is trained for another 3 epochs with fine-grained reports, using a cosine annealing scheduler for learning rate adjustments and a warmup phase for the first 10% of training steps. A batch size of 100 is maintained. The temperature parameters t are initialized to $\log 10$. The default hyperparameter λ is set to 0.5 and the default threshold for selecting high-confidence waveform features is set to 0.95. We use LLaMA3-8B (AI@Meta, 2024) as our LLM to query potential waveform features and use vLLM (Kwon et al., 2023) to speed up inference. All experiments used two NVIDIA A800 80GB GPUs, except LLaMA3-70B ablation, which used four.

Downstream Task Implementation: We evaluated the downstream tasks using both zero-shot and linear probe settings. For the zero-shot setting, we froze the entire model and used the text of each category as the prompt. We computed the similarity between the ECG embedding and the category text embedding as the classification probability. Additionally, we employed an ensemble method to enhance zero-shot performance. Specifically, in addition to using the category as text, we also added 'category in lead x' (x represents any of the 12 leads) as text to compute the probability and used the highest probability as the final probability for that category. For linear probing, we kept the ECG encoder frozen and updated only the parameters of a newly initialized linear classifier. We conducted linear probing for each task using 1%, 10%, and 100% of the training data. For all downstream tasks, we used macro AUC as the metric.

4.3 ZERO-SHOT ABILITY

The zero-shot results are illustrated in Table 1. Both CLEP and FG-CLEP performed well. A detailed examination of the data reveals that FG-CLEP significantly outperforms CLEP on PTBXL-Form, PTBXL-Rhythm demonstrating that continue training using fine-grained reports substantially enhanced the model's ability to capture local ECG waveform features. This improvement is particularly evident when using the ensemble method, which extends the label text to 12 leads ('label in lead

Table 1: Results of zero-shot classification. ENS: ensemble inference. FG-: trained with fine-grained reports.

macro AUC	PTB-XL-Super	PTBXL-Sub	PTBXL-Form	PTBXL-Rhythm	CPSC2018	CSN
METS (Li et al., 2024)	76.31	80.12	65.95	86.29	82.49	77.20
FG-METS	78.12↑1.81	82.01↑1.89	66.33↑0.38	90.12↑3.83	86.92↑4.43	81.20↑4.00
MERL (Liu et al., 2024b)	74.20	75.70	65.90	78.50	82.80	74.40
FG-MERL	76.70↑2.50	78.20↑2.50	66.80↑0.90	81.00↑2.50	85.30↑2.50	76.90↑2.50
MELP	76.20	81.20	69.10	85.40	84.20	77.60
D-BETA	76.20	75.90	66.10	88.60	80.10	76.30
CLEP	78.01	82.41	67.96	89.48	85.94	80.88
FG-CLEP	**80.13**↑2.12	**84.46**↑2.05	**68.46**↑0.50	**93.02**↑3.54	**88.90**↑2.96	**83.23**↑2.35
CLEP_{ENS}	76.26↓1.75	83.23↑0.82	65.71↓2.25	89.18↓0.30	84.72↓1.22	81.93↑1.05
$\text{FG-CLEP}_{\text{ENS}}$	**80.55**↑0.42	**84.42**↓0.04	**71.85**↑3.39	93.52↑0.50	87.93↓0.97	**85.58**↑2.35

Table 2: Results of Linear Evaluation.

Method	PTB-XL-Super			PTBXL-Sub			PTBXL-Form			PTBXL-Rhythm			CPSC2018			CSN		
	1%	10%	100%	1%	10%	100%	1%	10%	100%	1%	10%	100%	1%	10%	100%	1%	10%	100%
Random Init	70.45	77.09	81.61	55.82	67.60	77.91	55.82	62.54	73.00	46.26	62.36	79.29	54.96	71.47	78.33	47.22	63.17	73.13
SimCLR	63.41	69.77	73.53	60.84	68.27	73.39	54.98	56.97	62.52	51.41	69.44	77.73	59.78	68.52	76.54	59.02	67.26	73.20
BYOL	71.70	73.83	76.45	57.16	67.44	71.64	48.73	61.63	70.82	41.99	74.40	77.17	60.88	74.42	78.75	54.20	71.92	74.69
BarlowTwins	72.87	75.96	78.41	62.57	70.84	74.34	52.12	60.39	66.14	50.12	73.54	77.62	55.12	72.75	78.39	60.72	71.64	77.43
MoCo-v3	73.19	76.65	78.26	55.88	69.21	76.69	50.32	63.71	71.31	51.38	71.66	74.33	62.13	76.74	75.29	54.61	74.26	77.68
SimSiam	73.15	72.70	75.63	62.52	69.31	76.38	55.16	62.91	71.31	49.30	69.47	75.92	58.35	72.89	75.31	58.25	68.61	77.41
TS-TCC	70.73	75.88	78.91	53.54	66.98	77.87	48.04	61.79	71.18	43.34	69.48	78.23	57.07	73.62	78.72	55.26	68.48	76.79
CLOCS	68.94	73.36	76.31	57.94	72.55	76.24	51.97	57.96	72.65	47.19	71.88	76.31	59.59	77.78	77.49	54.38	71.93	76.13
ASTCL	72.51	77.31	81.02	61.86	68.77	76.51	44.14	60.93	66.99	52.38	71.98	76.05	57.90	77.01	79.51	56.40	70.87	75.79
CRT	69.68	78.24	77.24	61.98	70.82	78.67	46.41	59.49	68.73	47.44	73.52	74.41	58.01	76.43	82.03	56.21	73.70	78.80
ST-MEM	61.12	66.87	71.36	54.12	57.86	63.59	55.71	59.99	66.07	51.12	65.44	74.85	56.69	63.32	70.39	59.77	66.87	71.36
MELP	85.82	87.61	87.87	79.22	84.40	87.46	63.41	76.71	83.30	88.83	94.65	96.91	88.54	91.75	94.32	78.25	84.83	90.17
D-BETA	83.15	88.36	90.11	77.74	82.92	85.15	70.10	78.91	83.98	86.61	92.83	96.71	85.46	91.35	94.92	80.04	87.36	90.71
MERL	82.39	86.27	88.67	64.90	80.56	84.72	58.26	72.43	79.65	53.33	82.88	88.34	70.33	85.32	90.57	**66.60**	**82.74**	87.95
CLEP	84.73	89.45	90.24	69.61	**86.39**	92.86	68.64	73.23	83.27	62.39	**92.80**	90.81	83.79	94.02	97.22	63.54	80.76	94.01
FG-CLEP	**85.49**	**90.34**	**91.33**	**70.86**	86.46	**93.36**	**69.53**	**75.53**	**86.26**	**69.61**	92.11	**94.64**	**84.08**	**94.33**	**97.42**	63.32	80.01	**94.17**

x', where x represents any of the 12 leads). This further indicates FG-CLEP's fine-grained waveform feature capture capability. However, the ensemble inference method often proves detrimental to CLEP, as seen in PTBXL-Super, PTBXL-Form, and CPSC2018.

Additionally, we applied our generated fine-grained reports to other methods, METS (Li et al., 2024) and MERL (Liu et al., 2024b), to validate the generalizability. The results demonstrate that our fine-grained reports can also enhance the performance of these methods.

4.4 Linear Evaluation

We aim to evaluate the learned model transferability to downstream supervised tasks. We froze the ECG encoder and fine-tuned a randomly initialized linear classification head on the training data with binary cross-entropy loss. We compared a series of contrastive and generative self-supervised learning methods. Results in Table 2 show that FG-CLEP still achieves the best performances across all methods (Chen et al., 2020; Grill et al., 2020; Zbontar et al., 2021; Chen et al., 2021; Chen & He, 2021; Eldele et al., 2021; Kiyasseh et al., 2021; Wang et al., 2023; Zhang et al., 2023; Na et al., 2024; Liu et al., 2024b) in most scenarios.

Furthermore, when comparing the linear probe result in Table 2 with the zero-shot result in Table 1, we surprisingly find that FG-CLEP's zero-shot predictions are comparable to Linear Probe evaluations using 10% of the data in PTBXL-Sub, PTBXL-Form, CPSC2018, and CSN. Additionally, the zero-shot performance in PTBXL-Form is comparable to the full 100% Linear Probe evaluation. This further confirms the robustness and generalizability of our framework.

5 Analysis

In this section, we conduct a series of experiments to provide an in-depth analysis of FG-CLEP. The reported metrics reflect the average zero-shot AUC across the six datasets described above.

5.1 Ablation Study

To evaluate the effectiveness of our proposed fine-grained alignment with tag-specific ECG segments, the coarse-to-fine training with fine-grained reports, and the false negative mitigation loss function, we conducted a series of ablation studies. The results are presented in Table 3.

Table 3: Results of ablation study.

Model Setting	AUC
FG-CLEP(default)	83.03
w/o Fine-Grained Alignment	82.27
w/o Fine-Grained Report	80.78
CLEP + 3 epochs (original reports)	80.03
FG-CLEP (trained from scratch)	83.01
w/o False Negative Mitigation	81.67

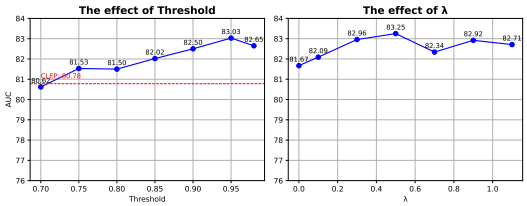

Figure 3: Effect of Threshold and λ.

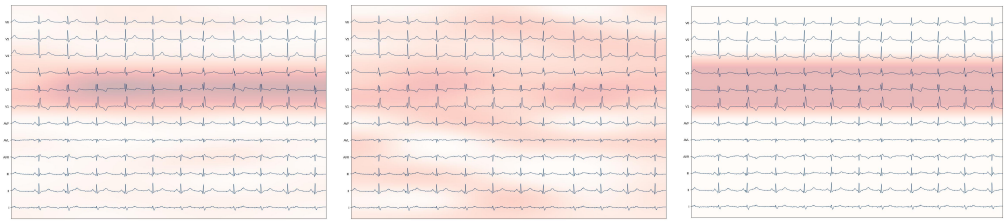

(a) Visual activation map of FG-CLEP (b) w/o fine-grained alignment (c) Clinical physician annotation

Figure 4: Visual activation maps generated by FG-CLEP and by the model without fine-grained alignment, using the text prompt *'RSR' Pattern in V1-V3'*.

Specifically, when removing the fine-grained alignment and performing contrastive learning only at the whole-report and ECG level, the performance drops significantly. We also compared FG-CLEP with CLEP trained without the additional 3 epochs of fine-grained report training. The results demonstrate that FG-CLEP significantly outperforms CLEP. To further confirm that the performance gains stem from the fine-grained reports rather than additional training epochs, we trained CLEP for 3 extra epochs using the original reports. The findings indicate that CLEP converges within 10 epochs, and the additional training even risks overfitting, leading to a slight performance drop. This further validates the importance of fine-grained reports. We also tested training FG-CLEP from scratch using fine-grained reports instead of continuing from CLEP. The results show no performance improvement but increased computational costs, supporting our default approach of continuing training from CLEP. Additionally, to verify the effectiveness of mitigating false negatives, we evaluated the performance without L_{fnm}. The results reveal a significant performance drop, highlighting the efficacy of our proposed loss function in addressing false negatives.

Finally, to assess the robustness of our method, we conducted ablation experiments on the loss hyperparameter λ and the threshold for selecting fine-grained waveform features. As shown in Figure 3, our model maintains strong performance across different λ and threshold values, demonstrating its robustness. To ensure high precision in generating waveform features, we set a relatively high default threshold of 0.95.

5.2 Visual Activation Map

To further demonstrate the fine-grained alignment between report tags and specific ECG segments, we present visual activation maps generated by FG-CLEP and by the model without fine-grained alignment using the text prompt 'RSR' Pattern in V1-V3', which is a key waveform feature for diagnosing right bundle branch block. As shown in Figure 4, FG-CLEP effectively captures ECG segments relevant to the text prompt, whereas the model without fine-grained alignment fails to accurately localize the specific ECG segments. This further validates the effectiveness of our approach in achieving fine-grained alignment.

5.3 Validation of Fine-Grained Report

In our training dataset MIMIC-ECG, nearly 50% of reports do not mention any waveform features. As mentioned earlier, rather than directly using the waveform features generated by the LLM as ground truth, we validate these features with CLEP to produce fine-grained reports. To evaluate the accuracy and reliability of the generated fine-grained reports, as well as the effectiveness of CLEP for validation, we randomly selected 100 ECGs that lacked waveform features. Three medical students independently annotated these ECGs for five key waveform features. The final labels

Table 4: AUC of Generated Fine-Grained Reports (with/without verification).

Waveform Feature	w/o Veri.	w Veri.
Non-specific ST elevation	71.42	83.42
Long QT-interval	84.25	93.25
Abnormal QRS	76.68	91.68
Prolonged PR interval	75.13	86.13
Inverted T-waves	74.79	88.79

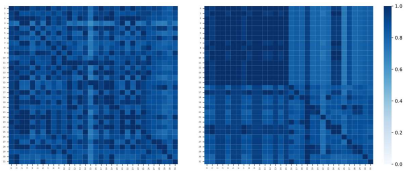

Figure 5: **The Heatmap of Semantic Similarity Matrix.** Left: a random batch; Right: with the first 16 as normal ECG and the last 16 as abnormal ECG.

were determined by majority vote, and the accuracy of the generated fine-grained reports was calculated accordingly. Since the same waveform feature may have different (granular) expressions, we computed the similarity between the generated reports and the five waveform features to obtain AUC values. As shown in Table 4, the AUC of waveform features directly generated by the LLM is relatively low, which aligns with expectations due to the hallucination issues of LLMs and the non-bijective relationship between ECG waveform features and diagnoses. However, after validation with CLEP, the AUC of the fine-grained reports improves significantly, demonstrating the effectiveness and reliability of the coarse-to-fine training process in generating fine-grained reports.

5.4 Semantic Similarity Matrix

We visualize the semantic similarity matrix in Figure 5. The left side shows the semantic similarity matrix from a random batch. As illustrated, ECGs and tags from different records may share similarities to some extent. Ignoring these similarities would result in a diagonal matrix with ones on the diagonal and zeros elsewhere, which is obviously wrong. The right side displays a semantic similarity matrix where the first 16 entries are normal ECGs and the last 16 are abnormal ECGs. The matrix effectively captures the semantic similarities of the normal ECGs.

5.5 Different Components

We conducted experiments to evaluate the performance of our framework using different LLMs and text encoders. The results are presented in Table 5. The findings indicate that our framework is robust across various components. Specifically, for different LLMs (Abdin et al., 2024; Jiang et al., 2023a; AI@Meta, 2024; Labrak et al., 2024; Ankit Pal, 2024), larger LLM provide some performance improvements, though the gains are not substantial. While domain-specific LLMs possess more medical knowledge, our method requires formatting the waveform feature outputs, an area where domain-specific models are less effective, resulting in performance that does not surpass general-purpose models. For different text encoders (Alsentzer et al., 2019; Gu et al., 2021; Jin et al., 2023; Lee et al., 2020), our framework consistently achieves significant improvements.

Table 5: Results on Different LLM/Text Encoder/ECG Encoder.

Model Type	CLEP	FG-CLEP ↑
Different LLMs		
LLaMA3-8B-Instruct	80.78	83.03
LLaMA3-70B-Instruct	80.78	83.42
Qwen3-8B	80.78	83.00
Phi-3-mini-4k-instruct	80.78	81.51
Mistral-7B-Instruct-v0.2	80.78	82.12
BioMistral-7B	80.78	82.67
LLaMA3-OpenBioLLM-8B	80.78	83.23
Different Text Encoders		
BioClinicalBERT	80.78	83.03
PubMedBERT	80.92	82.07
Med-CPT	78.55	81.21
BioBERT	78.63	81.20

6 Conclusion

In this paper, we introduced FG-CLEP, a fine-grained ECG-text contrastive learning framework that enhances waveform understanding by aligning specific ECG segments with report tags. Our coarse-to-fine training process leverages large language models to recover missing waveform features and incorporates a semantic similarity matrix to mitigate false negatives. Extensive experiments on six datasets demonstrate that FG-CLEP achieves state-of-the-art performance in both zero-shot and linear probing settings. These results highlight the effectiveness and generalizability of FG-CLEP.

REFERENCES

Marah Abdin, Sam Ade Jacobs, Ammar Ahmad Awan, Jyoti Aneja, Ahmed Awadallah, Hany Awadalla, Nguyen Bach, Amit Bahree, Arash Bakhtiari, Harkirat Behl, et al. Phi-3 technical report: A highly capable language model locally on your phone. *arXiv preprint arXiv:2404.14219*, 2024.

AI@Meta. Llama 3 model card. 2024. URL https://github.com/meta-llama/llama3/blob/main/MODEL_CARD.md.

Emily Alsentzer, John R Murphy, Willie Boag, Wei-Hung Weng, Di Jin, Tristan Naumann, and Matthew McDermott. Publicly available clinical bert embeddings. *arXiv preprint arXiv:1904.03323*, 2019.

Malaikannan Sankarasubbu Ankit Pal. Openbiollms: Advancing open-source large language models for healthcare and life sciences. https://huggingface.co/aaditya/OpenBioLLM-Llama3-70B, 2024.

Yehualashet Megersa Ayano, Friedhelm Schwenker, Bisrat Derebssa Dufera, and Taye Girma Debelee. Interpretable machine learning techniques in ecg-based heart disease classification: a systematic review. *Diagnostics*, 13(1):111, 2022.

Ting Chen, Simon Kornblith, Mohammad Norouzi, and Geoffrey Hinton. A simple framework for contrastive learning of visual representations. In *International conference on machine learning*, pp. 1597–1607. PMLR, 2020.

Xinlei Chen and Kaiming He. Exploring simple siamese representation learning. In *Proceedings of the IEEE/CVF conference on computer vision and pattern recognition*, pp. 15750–15758, 2021.

Xinlei Chen, Saining Xie, and Kaiming He. An empirical study of training self-supervised vision transformers. In *Proceedings of the IEEE/CVF international conference on computer vision*, pp. 9640–9649, 2021.

Alexey Dosovitskiy, Lucas Beyer, Alexander Kolesnikov, Dirk Weissenborn, Xiaohua Zhai, Thomas Unterthiner, Mostafa Dehghani, Matthias Minderer, Georg Heigold, Sylvain Gelly, et al. An image is worth 16x16 words: Transformers for image recognition at scale. *arXiv preprint arXiv:2010.11929*, 2020.

Emadeldeen Eldele, Mohamed Ragab, Zhenghua Chen, Min Wu, Chee Keong Kwoh, Xiaoli Li, and Cuntai Guan. Time-series representation learning via temporal and contextual contrasting. *arXiv preprint arXiv:2106.14112*, 2021.

Yunfan Gao, Yun Xiong, Xinyu Gao, Kangxiang Jia, Jinliu Pan, Yuxi Bi, Yixin Dai, Jiawei Sun, Haofen Wang, and Haofen Wang. Retrieval-augmented generation for large language models: A survey. *arXiv preprint arXiv:2312.10997*, 2(1), 2023.

Brian Gow, Tom Pollard, Larry A Nathanson, Alistair Johnson, Benjamin Moody, Chrystinne Fernandes, Nathaniel Greenbaum, Seth Berkowitz, Dana Moukheiber, Parastou Eslami, et al. Mimic-iv-ecg-diagnostic electrocardiogram matched subset.

Jean-Bastien Grill, Florian Strub, Florent Altché, Corentin Tallec, Pierre Richemond, Elena Buchatskaya, Carl Doersch, Bernardo Avila Pires, Zhaohan Guo, Mohammad Gheshlaghi Azar, et al. Bootstrap your own latent-a new approach to self-supervised learning. *Advances in neural information processing systems*, 33:21271–21284, 2020.

Yu Gu, Robert Tinn, Hao Cheng, Michael Lucas, Naoto Usuyama, Xiaodong Liu, Tristan Naumann, Jianfeng Gao, and Hoifung Poon. Domain-specific language model pretraining for biomedical natural language processing. *ACM Transactions on Computing for Healthcare (HEALTH)*, 3(1): 1–23, 2021.

Serkan Günay, Ahmet Öztürk, and Yavuz Yiğit. The accuracy of gemini, gpt-4, and gpt-4o in ecg analysis: A comparison with cardiologists and emergency medicine specialists. *The American journal of emergency medicine*, 84:68–73, 2024.

Rui Hu, Jie Chen, and Li Zhou. Spatiotemporal self-supervised representation learning from multi-lead ecg signals. *Biomedical Signal Processing and Control*, 84:104772, 2023.

Lei Huang, Weijiang Yu, Weitao Ma, Weihong Zhong, Zhangyin Feng, Haotian Wang, Qianglong Chen, Weihua Peng, Xiaocheng Feng, Bing Qin, et al. A survey on hallucination in large language models: Principles, taxonomy, challenges, and open questions. *ACM Transactions on Information Systems*, 2023.

Albert Q Jiang, Alexandre Sablayrolles, Arthur Mensch, Chris Bamford, Devendra Singh Chaplot, Diego de las Casas, Florian Bressand, Gianna Lengyel, Guillaume Lample, Lucile Saulnier, et al. Mistral 7b. *arXiv preprint arXiv:2310.06825*, 2023a.

Chaoya Jiang, Wei Ye, Haiyang Xu, Shikun Zhang, Jie Zhang, Fei Huang, et al. Vision lanauge pre-training by contrastive learning with cross-modal similarity regulation. *arXiv preprint arXiv:2305.04474*, 2023b.

Jill Jin. Screening for cardiovascular disease risk with ecg. *Jama*, 319(22):2346–2346, 2018.

Qiao Jin, Won Kim, Qingyu Chen, Donald C Comeau, Lana Yeganova, W John Wilbur, and Zhiyong Lu. Medcpt: Contrastive pre-trained transformers with large-scale pubmed search logs for zero-shot biomedical information retrieval. *Bioinformatics*, 39(11):btad651, 2023.

Myunsoo Kim, Seong-Woong Shim, and Byung-Jun Lee. Falcon: False-negative aware learning of contrastive negatives in vision-language pretraining. *arXiv preprint arXiv:2505.11192*, 2025.

Dani Kiyasseh, Tingting Zhu, and David A Clifton. Clocs: Contrastive learning of cardiac signals across space, time, and patients. In *International Conference on Machine Learning*, pp. 5606–5615. PMLR, 2021.

Woosuk Kwon, Zhuohan Li, Siyuan Zhuang, Ying Sheng, Lianmin Zheng, Cody Hao Yu, Joseph E. Gonzalez, Hao Zhang, and Ion Stoica. Efficient memory management for large language model serving with pagedattention. In *Proceedings of the ACM SIGOPS 29th Symposium on Operating Systems Principles*, 2023.

Yanis Labrak, Adrien Bazoge, Emmanuel Morin, Pierre-Antoine Gourraud, Mickael Rouvier, and Richard Dufour. Biomistral: A collection of open-source pretrained large language models for medical domains. *arXiv preprint arXiv:2402.10373*, 2024.

Sravan Kumar Lalam, Hari Krishna Kunderu, Shayan Ghosh, Harish Kumar, Samir Awasthi, Ashim Prasad, Francisco Lopez-Jimenez, Zachi I Attia, Samuel Asirvatham, Paul Friedman, et al. Ecg representation learning with multi-modal ehr data. *Transactions on Machine Learning Research*, 2023.

Samuel Lavoie, Polina Kirichenko, Mark Ibrahim, Mahmoud Assran, Andrew Gordon Wildon, Aaron Courville, and Nicolas Ballas. Modeling caption diversity in contrastive vision-language pretraining. *arXiv preprint arXiv:2405.00740*, 2024.

Jinhyuk Lee, Wonjin Yoon, Sungdong Kim, Donghyeon Kim, Sunkyu Kim, Chan Ho So, and Jaewoo Kang. Biobert: a pre-trained biomedical language representation model for biomedical text mining. *Bioinformatics*, 36(4):1234–1240, 2020.

Jun Li, Che Liu, Sibo Cheng, Rossella Arcucci, and Shenda Hong. Frozen language model helps ecg zero-shot learning. In *Medical Imaging with Deep Learning*, pp. 402–415. PMLR, 2024.

Zheng Li, Caili Guo, Zerun Feng, Jenq-Neng Hwang, and Zhongtian Du. Integrating language guidance into image-text matching for correcting false negatives. *IEEE Transactions on Multimedia*, 2023.

Xinjie Liang, Xiangyu Li, Fanding Li, Jie Jiang, Qing Dong, Wei Wang, Kuanquan Wang, Suyu Dong, Gongning Luo, and Shuo Li. Medfilip: Medical fine-grained language-image pre-training. *IEEE Journal of Biomedical and Health Informatics*, 2025.

Che Liu, Zhongwei Wan, Sibo Cheng, Mi Zhang, and Rossella Arcucci. Etp: Learning transferable ecg representations via ecg-text pre-training. In *ICASSP 2024-2024 IEEE International Conference on Acoustics, Speech and Signal Processing (ICASSP)*, pp. 8230–8234. IEEE, 2024a.

Che Liu, Zhongwei Wan, Cheng Ouyang, Anand Shah, Wenjia Bai, and Rossella Arcucci. Zero-shot ecg classification with multimodal learning and test-time clinical knowledge enhancement. *arXiv preprint arXiv:2403.06659*, 2024b.

Feifei Liu, Chengyu Liu, Lina Zhao, Xiangyu Zhang, Xiaoling Wu, Xiaoyan Xu, Yulin Liu, Caiyun Ma, Shoushui Wei, Zhiqiang He, et al. An open access database for evaluating the algorithms of electrocardiogram rhythm and morphology abnormality detection. *Journal of Medical Imaging and Health Informatics*, 8(7):1368–1373, 2018.

Yeongyeon Na, Minje Park, Yunwon Tae, and Sunghoon Joo. Guiding masked representation learning to capture spatio-temporal relationship of electrocardiogram. *arXiv preprint arXiv:2402.09450*, 2024.

Bo Ni, Zheyuan Liu, Leyao Wang, Yongjia Lei, Yuying Zhao, Xueqi Cheng, Qingkai Zeng, Luna Dong, Yinglong Xia, Krishnaram Kenthapadi, et al. Towards trustworthy retrieval augmented generation for large language models: A survey. *arXiv preprint arXiv:2502.06872*, 2025.

Hung Manh Pham, Aaqib Saeed, and Dong Ma. Boosting masked ecg-text auto-encoders as discriminative learners. *arXiv preprint arXiv:2410.02131*, 2024.

Alec Radford, Jong Wook Kim, Chris Hallacy, Aditya Ramesh, Gabriel Goh, Sandhini Agarwal, Girish Sastry, Amanda Askell, Pamela Mishkin, Jack Clark, et al. Learning transferable visual models from natural language supervision. In *International conference on machine learning*, pp. 8748–8763. PMLR, 2021.

Adyasha Rath, Debahuti Mishra, Ganapati Panda, and Suresh Chandra Satapathy. Heart disease detection using deep learning methods from imbalanced ecg samples. *Biomedical Signal Processing and Control*, 68:102820, 2021.

S Sahoo, M Dash, S Behera, and S Sabut. Machine learning approach to detect cardiac arrhythmias in ecg signals: A survey. *Irbm*, 41(4):185–194, 2020.

Zhongyi Shui, Jianpeng Zhang, Weiwei Cao, Sinuo Wang, Ruizhe Guo, Le Lu, Lin Yang, Xianghua Ye, Tingbo Liang, Qi Zhang, et al. Large-scale and fine-grained vision-language pre-training for enhanced ct image understanding. *arXiv preprint arXiv:2501.14548*, 2025.

Weixuan Sun, Jiayi Zhang, Jianyuan Wang, Zheyuan Liu, Yiran Zhong, Tianpeng Feng, Yandong Guo, Yanhao Zhang, and Nick Barnes. Learning audio-visual source localization via false negative aware contrastive learning. In *Proceedings of the IEEE/CVF Conference on Computer Vision and Pattern Recognition*, pp. 6420–6429, 2023.

Patrick Wagner, Nils Strodthoff, Ralf-Dieter Bousseljot, Dieter Kreiseler, Fatima I Lunze, Wojciech Samek, and Tobias Schaeffter. Ptb-xl, a large publicly available electrocardiography dataset. *Scientific data*, 7(1):154, 2020.

Fuying Wang, Jiacheng Xu, and Lequan Yu. From token to rhythm: A multi-scale approach for ecg-language pretraining. *arXiv preprint arXiv:2506.21803*, 2025.

Ning Wang, Panpan Feng, Zhaoyang Ge, Yanjie Zhou, Bing Zhou, and Zongmin Wang. Adversarial spatiotemporal contrastive learning for electrocardiogram signals. *IEEE Transactions on Neural Networks and Learning Systems*, 2023.

Zifeng Wang, Zhenbang Wu, Dinesh Agarwal, and Jimeng Sun. Medclip: Contrastive learning from unpaired medical images and text. *arXiv preprint arXiv:2210.10163*, 2022.

Jason Wei, Xuezhi Wang, Dale Schuurmans, Maarten Bosma, Fei Xia, Ed Chi, Quoc V Le, Denny Zhou, et al. Chain-of-thought prompting elicits reasoning in large language models. *Advances in neural information processing systems*, 35:24824–24837, 2022.

Han Yu, Peikun Guo, and Akane Sano. Ecg semantic integrator (esi): A foundation ecg model pretrained with llm-enhanced cardiological text. *arXiv preprint arXiv:2405.19366*, 2024.

Jure Zbontar, Li Jing, Ishan Misra, Yann LeCun, and Stéphane Deny. Barlow twins: Self-supervised learning via redundancy reduction. In *International conference on machine learning*, pp. 12310–12320. PMLR, 2021.

Xiaohua Zhai, Basil Mustafa, Alexander Kolesnikov, and Lucas Beyer. Sigmoid loss for language image pre-training. In *Proceedings of the IEEE/CVF International Conference on Computer Vision*, pp. 11975–11986, 2023.

Huaicheng Zhang, Wenhan Liu, Jiguang Shi, Sheng Chang, Hao Wang, Jin He, and Qijun Huang. Maefe: Masked autoencoders family of electrocardiogram for self-supervised pretraining and transfer learning. *IEEE Transactions on Instrumentation and Measurement*, 72:1–15, 2022a.

Wenrui Zhang, Ling Yang, Shijia Geng, and Shenda Hong. Self-supervised time series representation learning via cross reconstruction transformer. *arXiv preprint arXiv:2205.09928*, 2022b.

Wenrui Zhang, Ling Yang, Shijia Geng, and Shenda Hong. Self-supervised time series representation learning via cross reconstruction transformer. *IEEE Transactions on Neural Networks and Learning Systems*, 2023.

Yue Zhang, Yafu Li, Leyang Cui, Deng Cai, Lemao Liu, Tingchen Fu, Xinting Huang, Enbo Zhao, Yu Zhang, Yulong Chen, et al. siren's song in the ai ocean: A survey on hallucination in large language models. *Computational Linguistics*, pp. 1–46, 2025.

J Zheng, H Guo, and H Chu. A large scale 12-lead electrocardiogram database for arrhythmia study (version 1.0. 0). *PhysioNet 2022Available online: http://physionet. org/content/ecg-arrhythmia/1.0. 0/(accessed on 23 November 2022)*, 2022.

A Dataset Analysis

We pre-train the FG-CLEP using the MIMIC-ECG dataset and test it on the PTB-XL, CPSC2018, and CSN datasets. All the ECGs in the datasets are 12-lead recordings. The PTB-XL dataset can be further divided into four subsets, and we follow the official train:validation:test split. For CPSC2018 and CSN, we split the dataset as 70%:10%:20% for the train:validation:test split. The statistics of the datasets used are presented in Table 6.

MIMIC-ECG The MIMIC-ECG dataset contains nearly 800,000 ECG-report pairs from approximately 160,000 unique patients. These diagnostic ECGs utilize 12 leads and are 10 seconds in duration, with a sampling rate of 500 Hz.

PTB-XL The PTB-XL ECG dataset is a large dataset of 21,799 clinical 12-lead ECGs from 18,869 patients of 10-second length. There are four subsets with multi-label classification tasks: Superclass (5 categories), Subclass (23 categories), Form (19 categories), and Rhythm (12 categories). Notably, these four subsets have different numbers of samples.

CPSC2018 This publicly accessible dataset comprises 6,877 standard 12-lead ECG records, each sampled at a rate of 500 Hz, with durations ranging from 6 to 60 seconds. The dataset is annotated with 9 distinct labels.

Chapman-Shaoxing-Ningbo (CSN) This dataset contains 12-lead ECGs of 45,152 patients with a 500 Hz sampling rate. It features multiple common rhythms and additional cardiovascular conditions, all labeled by professional experts.

B Pseudo Code

The pseudo-code of our FG-CLEP training process is shown in algorithm 1

Table 6: The statistics of used datasets.

Pretrain	**# ECGs**	**# Reports**		
MIMIC-ECG	773,268	773,268		
Evaluation	**# Train**	**# Valid**	**# Test**	**# Classes**
PTB-XL Super	17,084	2,146	2,158	5
PTB-XL Sub	17,084	2,146	2,158	23
PTB-XL Form	7,197	901	880	19
PTB-XL Rhythm	16,832	2,100	2,098	12
CPSC2018	4,800	684	1,383	9
CSN	31,606	4,515	9,031	51

Algorithm 1 FG-CLEP Training Process

Input: $D = \{(x_{\text{ecg}_i}, x_{\text{txt}_i}) \mid i \in [0, n)\}$
Output: FG-CLEP
Perform contrastive training on CLEP using D
Generate fine-grained reports
for $i = 0$ to $n - 1$ **do**
    $f_{\text{features}} = \text{LLM}(x_{\text{txt}_i}, \text{prompt})$
    for $j = 1$ to m **do**
        where m is the number of waveform features generated
        $\text{sim} = \text{CLEP}(x_{\text{ecg}_i}, f_j)$
        if sim $>$ threshold **then**
            $x_{\text{txt}_i} = x_{\text{txt}_i} + f_j$
        end if
    end for
end for
Continue training CLEP on $\{(x_{\text{ecg}_i}, x_{\text{txt}_i})\}$ to obtain FG-CLEP

C Running Cases for Generating Fine-Grained Reports

We present three case studies illustrating how the fine-grained reports with waveform features are generated step by step, as shown in Figure 6, 7, 8. The LLM is prompted with two explicit chain-of-thought instructions: **'What waveform features are most likely to be present in electrocardiograms with these symptoms?'** followed by **'Organize these waveform features into a Python list, with each item representing a distinct waveform feature.'**

D ECG-Text Retrieval

We attempted to use FG-CLEP to retrieve electrocardiograms (ECGs) from the MIMIC-ECG dataset (Gow et al.) through text. To test our model's ability to capture fine-grained waveform features, we tested a series of typical waveform features such as 'RSR' Pattern, 'Inverted T-waves,' and 'Low QRS voltages.' Figure 9 shows the Top 3 retrieved ECGs with probabilities all greater than 0.99. Our model demonstrated strong capability in retrieving ECGs through waveform feature text, which can lead to two applications: (1) Helping doctors quickly find similar cases or specific ECG patterns, aiding in diagnosis and treatment decision-making; (2) In medical education, text-based retrieval can quickly find typical ECG cases, assisting in teaching and training, thereby improving educational effectiveness.

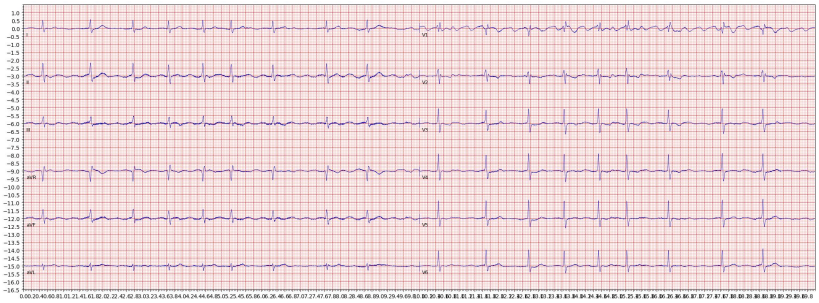

ID: p14578883/s43946433/43946433
Report: Atrial fibrillation., Right bundle branch block, Abnormal ECG
LLM Output:
Here is the list of waveform features organized into a Python list:

```
waveform_features = [
    "Irregularly irregular rhythm",
    "Absent or fragmented P-waves",
    "Wide QRS complexes (>120 ms)",
    "Variable RR intervals",
    "Fibrillatory waves (f-waves) or oscillations",
    "Wavy or sawtooth pattern",
    "Notched or slurred R wave in leads I, II, and V5-V6",
    "Inverted or absent R wave in lead V1",
    "Delta wave (slurred upstroke of the QRS complex) in leads I, II, and V5-V6",
    "RSR' pattern in leads V1-V3",
    "ST segment changes (elevation, depression, or inversion)",
    "T wave changes (inversion, flattening, or peaking)",
    "QT interval prolongation or shortening",
    "PR interval prolongation or shortening",
    "U waves or other abnormal waveforms"
]
```

Note that this list is not exhaustive, and there may be other waveform features that are not included here. Additionally, the presence of these features does not necessarily confirm a specific diagnosis, and further evaluation and testing may be necessary to establish a definitive diagnosis.
Potential Waveform features:
['Irregularly irregular rhythm', 'Absent or fragmented P-waves', 'Wide QRS complexes (>120 ms)', 'Variable RR intervals', 'Fibrillatory waves (f-waves) or oscillations', 'Wavy or sawtooth pattern', 'Notched or slurred R wave in leads I, II, and V5-V6', 'Inverted or absent R wave in lead V1', 'Delta wave (slurred upstroke of the QRS complex) in leads I, II, and V5-V6', "RSR' pattern in leads V1-V3", 'ST segment changes (elevation, depression, or inversion)', 'T wave changes (inversion, flattening, or peaking)', 'QT interval prolongation or shortening', 'PR interval prolongation or shortening', 'U waves or other abnormal waveforms']
Probility:
[0.985297, 0.49500474, 0.95943975, 0.9952996, 0.96285915, 0.84171605, 0.88279337, 0.9455562, 0.98828167, 0.99366695, 0.62816966, 0.9148475, 0.99069655, 0.049276203, 0.9565827]
Fine-Grained Report: Atrial fibrillation., Right bundle branch block, Abnormal ECG, Irregularly irregular rhythm,Wide QRS complexes (>120 ms),Variable RR intervals,Fibrillatory waves (f-waves) or oscillations,Delta wave (slurred upstroke of the QRS complex) in leads I, II, and V5-V6,RSR' pattern in leads V1-V3,QT interval prolongation or shortening,U waves or other abnormal waveforms

Figure 6: Running Case1 with Atrial fibrillation and Right bundle branch block.

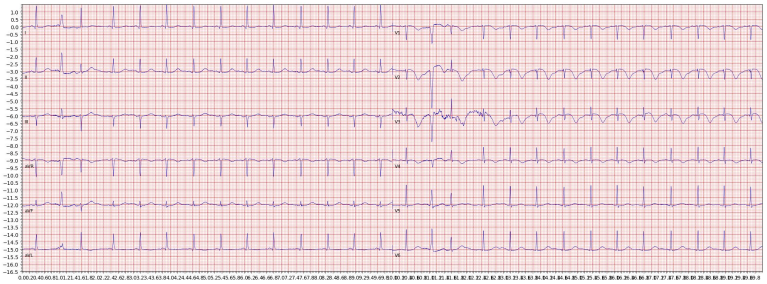

ID: p11799366/s45322712/45322712
Report: Probable atrial fibrillation, ventricular couplets, Long QTc interval, Ant/septal+lateral ST-T changes suggest myocardial infarction, Repolarization changes may be partly due to rhythm, Abnormal ECG
LLM Output:
Here is the list of waveform features organized in a Python list:

```
waveform_features = [
    "Irregularly irregular rhythm",
    "Absent or fragmented P waves",
    "Fibrillatory waves (f-waves) or oscillations in the atrial region",
    "Premature ventricular contractions (PVCs) with a different morphology from the normal QRS complex",
    "Ventricular couplets: two consecutive PVCs with a normal QRS complex in between",
    "Long QTc interval (> 440 ms for men, > 460 ms for women)",
    "Abnormal T-wave morphology (e.g., 'saddle-shaped' or 'inverted' T-wave)",
    "ST-segment elevation or depression in anteroseptal and lateral leads (e.g., V1-V3, I, aVL)",
    "T-wave inversion or abnormal T-wave morphology in anteroseptal and lateral leads",
    "Abnormal QRS complex morphology (e.g., wide or bizarre QRS complexes)",
    "Prolonged PR interval",
    "Abnormal QRS axis"
]
```

Note that I've kept the descriptions concise and focused on the key features, as they would be in a clinical setting.
Potential Waveform features:
['Irregularly irregular rhythm', 'Absent or fragmented P waves', 'Fibrillatory waves (f-waves) or oscillations in the atrial region', 'Premature ventricular contractions (PVCs) with a different morphology from the normal QRS complex', 'Ventricular couplets: two consecutive PVCs with a normal QRS complex in between', 'Long QTc interval (> 440 ms for men, > 460 ms for women)', "Abnormal T-wave morphology (e.g., 'saddle-shaped' or 'inverted' T-wave)", 'ST-segment elevation or depression in anteroseptal and lateral leads (e.g., V1-V3, I, aVL)', 'T-wave inversion or abnormal T-wave morphology in anteroseptal and lateral leads', 'Abnormal QRS complex morphology (e.g., wide or bizarre QRS complexes)', 'Prolonged PR interval', 'Abnormal QRS axis']
Probility:
[0.9616148, 0.9832206, 0.9936021, 0.9954572, 0.9854593, 0.99531144, 0.9919208, 0.9786107, 0.99453413, 0.99271095, 0.27789757, 0.51983744]
Fine-Grained Report: Probable atrial fibrillation, ventricular couplets, Long QTc interval, Ant/septal+lateral ST-T changes suggest myocardial infarction, Repolarization changes may be partly due to rhythm, Abnormal ECG, Irregularly irregular rhythm,Absent or fragmented P waves,Fibrillatory waves (f-waves) or oscillations in the atrial region,Premature ventricular contractions (PVCs) with a different morphology from the normal QRS complex,Ventricular couplets: two consecutive PVCs with a normal QRS complex in between,Long QTc interval (> 440 ms for men, > 460 ms for women),Abnormal T-wave morphology (e.g., 'saddle-shaped' or 'inverted' T-wave),ST-segment elevation or depression in anteroseptal and lateral leads (e.g., V1-V3, I, aVL),T-wave inversion or abnormal T-wave morphology in anteroseptal and lateral leads,Abnormal QRS complex morphology (e.g., wide or bizarre QRS complexes)

Figure 7: Running Case2 with Myocardial Infarction.

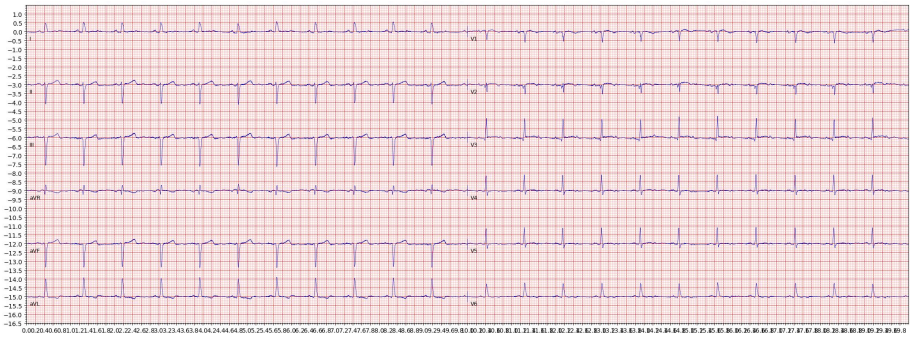

ID: p10474653/s42221714/42221714
Report: Sinus rhythm, Left anterior fascicular block, Possible septal infarct - age undetermined, Left ventricular hypertrophy, Lateral T wave changes are probably due to ventricular hypertrophy, Abnormal ECG
LLM Output:
Here is the list of waveform features organized in a Python list:

```
waveform_features = [
    "Sinus rhythm",
    "Left axis deviation (LAD) >30 ° ",
    "Q waves in leads I, II, or V5-V6",
    "ST segment depression in leads I, II, or V5-V6",
    "T wave inversion in leads I, II, or V5-V6",
    "Increased amplitude of the QRS complex (>3.5 mm) in leads I, II, or V5-V6",
    "Increased duration of the QRS complex (>120 ms)",
    "Deep S waves in leads I, II, or V5-V6",
    "T wave inversion or flattening in leads I, aVL, V5, and V6",
    "ST segment elevation or depression in other leads",
    "Prolonged QT interval",
    "Abnormal P wave morphology or axis"
]
```

Note that I've tried to be as specific as possible when describing each waveform feature, but some features may overlap or be related to each other.
Potential Waveform features:
['Sinus rhythm', 'Left axis deviation (LAD) >30 ° ', 'Q waves in leads I, II, or V5-V6', 'ST segment depression in leads I, II, or V5-V6', 'T wave inversion in leads I, II, or V5-V6', 'Increased amplitude of the QRS complex (>3.5 mm) in leads I, II, or V5-V6', 'Increased duration of the QRS complex (>120 ms)', 'Deep S waves in leads I, II, or V5-V6', 'T wave inversion or flattening in leads I, aVL, V5, and V6', 'ST segment elevation or depression in other leads', 'Prolonged QT interval', 'Abnormal P wave morphology or axis']
Probility:
[0.9861351, 0.5359271, 0.33153382, 0.71545005, 0.49900547, 0.42786044, 0.61200434, 0.18875751, 0.8920379, 0.78382677, 0.88176095]
Fine-Grained Report: Sinus rhythm, Left anterior fascicular block, Possible septal infarct - age undetermined, Left ventricular hypertrophy, Lateral T wave changes are probably due to ventricular hypertrophy, Abnormal ECG, Left axis deviation (LAD) >30 °

Figure 8: Running Case3 with Hypertrophy.

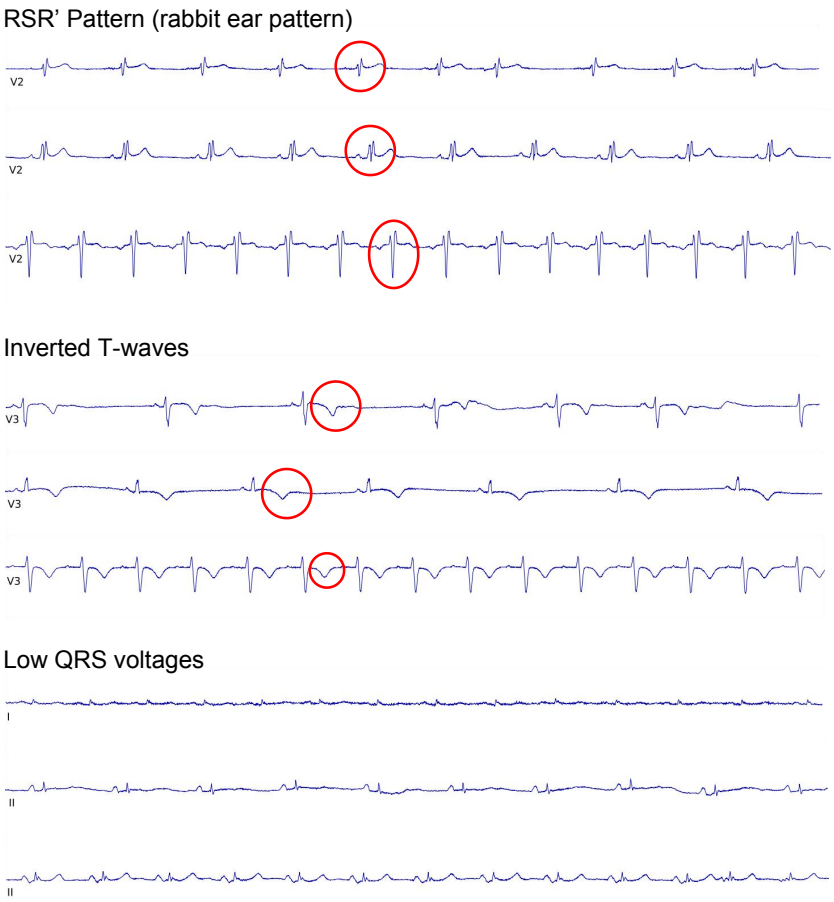

Figure 9: Top 3 retrieved ECG using FG-CLEP.